Research Article **www.ijcps.com**

International Journal of Chemical and Pharmaceutical Sciences
2015, June., Vol. 6 (2)

ISSN: 0976-9390
IJCPS

Photocatalytic degradation of pathogenic bacteria using Novel-composite ZnO nanofilms with 2-2' 1, 3-dithiolan-2-ylidenemethanediyl) diquinoline-4-carboxylic acid

[1] Ravi HR*, [2] Prashanth kumar PN, [3] Naveenkumar P, [4] Devarajegowda HC and [5] Sreepad HR.

[1] PG Department of Physics and Research Centre, BETAHE, Bharathicollege, Bharthinagara, Mandya, Karnataka, India.

[2] Department of Industrial Chemistry, Kuvempu University, Shankaraghatta, Karnataka, India.

[3] Department of Electronics, Yuvaraja's College (Autonomous), University of Mysore, Mysore, Karnataka, India.

[4] Department of Physics, yuvaraja's College (Autonomous), University of Mysore, Mysore, Karnataka, India.

[5] Research Centre, PG Department of Physics, GFG College, Mandya, Karnataka, India.

* **Corresponding Author:** E-Mail: ravihr1@yahoo.in

Received: 12th June 2015, Revised and Accepted: 14th June 2015

ABSTRACT

This paper presents the high bacterial interaction strategy to improve the antimicrobial activity of visible-light-activated ZnO films. The manufacturing nanostructured semiconductor layers on the glass substrates prepared from the surfactant-assisted complex sol–gel method obtained different grain sized Zinc Oxide (ZnO) nanoparticles using zinc nitrate and citric acid as starting material. The effect of the citric acid concentration, varying the pH of the sol solution and PEG 2000 surfactant which affects the grain size of the ZnO nanoparticles. It was investigated using X-ray diffraction and UV-Visible absorbance spectroscopy. In this study, we demonstrated that functionalized Zinc oxide substrates having superior visible-light-induced bactericidal activity against Escherichia coli compared to pure Zinc oxide films. Particularly at pH=1 ZnO nano films surface complexed by 1,3-dithiolan-2-ylidenemethanediyl)diquinoline-4-carboxylic acid supports for shifting the wavelength towards higher region then the other pH values (3,5,7) which is mainly due to the smaller the grain size and rich in surface active sites which affects the adsorption of dyes. For obtaining the high photocatalytic performance is attributed to an effect of following factors: rich in active surface area of the ZnO films, an increase in absorption and shifting the wavelength towards visible region of the functionalized semiconducting films, From these findings suggest that ZnO functionalized films has potential applications in the development of alternative disinfections for environmental usages.

Keywords: ZnO nanocrystalline films, novel sensitizer, Photocatalytic degradation of E-Coli bacteria.

1. INTRODUCTION

Semiconductor-mediated photocatalytic oxidation is regarded as a promising method for environmental decontamination. Among the semiconductors employed, ZnO is considered as a good photocatalyst because of its high photosensitivity, non-toxicity, easy availability, strong oxidizing power and long-term stability [1, 2]. Recently, there is a growing interest in photo-catalyst based on dye-sensitized semiconductor films [3].In most cases the low cost materials and high demand for renewable energy sources have increased the use of dye sensitized solar cells. Numerous efforts have been done by several research groups all over the world to utilize natural dyes as sensitizers in dye-sensitized solar cells. A photo electrochemical cell utilizing flavonoid and anthocyanin dyes extracted from blackberries along with colloidal TiO_2 powder, was reported to convert sunlight to electrical

power at an efficiency of 0.56% under full sun light [4].

Heterostructures are formed by quantum-sized ZnO nanocrystals and photosynthetic pigments were prepared by adsorbing either chlorophyll, carotenoids or their mixture onto a film of organic-capped ZnO nanoparticles and were studied in the photo electrochemical processes. The photo conversion process was found to be greatly enhanced at the nanocrystalline electrodes upon sensitization with a dye mixture [5]. Chlorophyll derivatives and related natural porphyrins were used in photosensitization of titania solar cells [6]. Zinc oxide semiconductor was coated with extracts of natural pigments, chlorophyll or anthocyanin and used for the photo bleaching of rose bengal dye [7]. Sensitized TiO_2 was used in water purification in order to photodegraded organic pollutants such as Methyl Orange and Phenazpyridine [8]. Since Fujishima and Honda [9] reported the photocatalytic properties of TiO_2 in 1972, semiconductor photocatalysis has received a lot of attention [10,11]. For instance, Lactobacillus acidophilus, Saccha-romyces cerevisiae, and Escherichia coli were completely sterilized when incubated with platinum-loaded TiO_2 under metal halide lamp irradiation for 60–120 mins [12,13]. TiO_2 photocatalysis is known to generate various active oxygen species, such as hydroxyl radicals, hydrogen peroxide, superoxide radical anions, etc., by redox reactions under UV irradiation whereas ZnO also generates active oxygen species [14], which was responsible for inhibition of bactericidal growth. Such films, having large band gap semiconductors have been investigated, which themselves absorb only in the lower wavelength UV region. The ZnO photocatalyst is effective only upon irradiation by UV light at levels that would induce serious damage to human cells. This greatly restricts the potential applications of ZnO substrates for use in our living environments. Although solar energy is inexhaustible, only a few percent of its energy are in the UV range. ZnO cannot be an effective bactericidal medium unless there is sufficient irradiation time under bright sunlight. For offering the potential to overcome this problem an alternative method is necessary to enabling efficient harvesting of visible light. For harvesting the dyes that should be selected to get desired broad, strong absorption over the visible and near-infrared wavelength range. Hence, surface functionalization of metal oxide wide band gap semiconductor surfaces by covalently attaching transition-metal complexes or organic sensitizers are central in applications for degradation of organic compounds, solar energy conversion by dye-sensitized solar cells and degradation of micro organisms [13-19].

However, most dyes are photochemically unstable and may not be able to absorb light in the desired wavelength range. Since 99% of the energy output from the sun is in the visible range, it is desirable for photosensitizers for sunlight-mediated disinfection to absorb visible light. For medical applications, absorbance in the near-infrared range is desirable, as these wavelengths penetrate more deeply into tissues than visible light. To adsorb these sensitizers it requires sufficient surface area of nanocrystalline ZnO films. Hence this chapter presents various sized ZnO nanoparticles was prepared by surfactant-assisted complex sol–gel method. The controlled preparation of zinc oxide (ZnO) nanoparticles using zinc nitrate and citric acid as starting material. ZnO nanoparticles with a pure wurtzite structure were obtained after calcination at 773 K. The effects of varying the pH of the sol solution, the optimized citric acid concentration, and the PEG-2000 surfactant controlled the average particle size of the ZnO nanoparticles was investigated by X-ray diffraction and UV-Visible spectrophotometer. The obtained various sized ZnO nanoparticles were coated on soda-lime glass substrate by previous technique .i.e. doctor blade method. For investigation the performances of photocatalytic inactivation achieved by smaller grain sized ZnO film is better than that larger grain sized ZnO nanocrystalline coated samples, which as a result it because smaller grain size that was directly proportional to larger surface area, as a result it offers higher chemisorbtion of dyes over monolayer ZnO films.

The principle of functionalised ZnO photosensitization is illustrated in Scheme 1, which indicates the primary electron pathway [20]. When a dye molecule absorbs visible light, it is excited to a higher energy state. The excited dye* then injects an electron to the conduction band of ZnO. The injected electron is scavenged by the surface-adsorbed O_2 to yield O_2^- and subsequently the OH radicals are responsible for bacterial inhibition growth. To the best of our knowledge Sondos Othman Abed-Alhadi Ateeq. et.al. [21] as recently, reported the investigation of anthocyanin sensitized ZnO catalyst in water containing E.coli bacteria. Hence, this paper introduces a novel class of (dithiolan-2-ylidenemethanediyl)diquinoline-4-carboxylic acid anchoring on ZnO nanocrystalline films, which was used for analyzing the bactericidal activities, It was found that the films can kill E.coli (ATCC 25922) bacteria under visible light irradiation 3> 420 nm) , effectively. Therefore we found that the higher photocatalytic inactivation achieved with pH =1 of ZnO coated film was better than that of other pH levels of ZnO-coated functionalized samples.

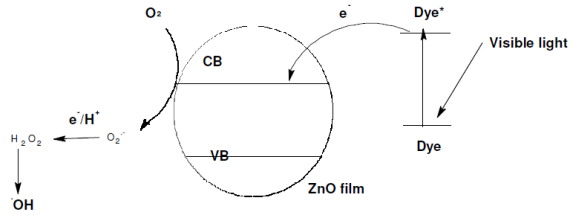

Scheme – 1

2. EXPERIMENTAL

2.1. Materials

Zn (NO3)2.6H2O, PEG-2000 surfactant, Isatin, Acetyl acetone, carbon disulphide and potassium carbonate. All the chemicals were purchased from Himedia laboratory and the reagents are analytical grade, and no needed for further purification.

2.2. Spectral measurements

The 1H NMR spectra were recorded on a Varian Gemini 300 (MHz) spectrometer; Mass spectra were recorded on LCMS-2010A SHIMADZU, UV-Visible spectrophotometer Shimadzu was used for optical absorbance measurements (UV-1650 model) , IR spectra (nominal 4-cm-1 resolution) were measured using a Digilab FTS-40 spectrometer, the dye powders were held in KBr pellets in the case of S1 sensitizers, whereas the sensitizers chemisorbed on semiconducting oxide films were measured using an attenuated total reflectance Infra red (ATR-IR) spectroscopy.

2.3. Synthesis of α α'-diacetyl ketene-(S,S)-acetals

The synthesis and application of α α'-oxo ketene-(S,S)-acetals have been reported elsewhere [22], Following the same procedure described in the literature α α'-oxo ketene-(S,S)-acetals were easily prepared from acetylacetone, carbon disulfide,1,2-dibromoethane in the presence of K2CO3 and DMF in nearly quantitative yields, respectively. Yield 86%, M.P (°C) = 156–158).

2.4. Synthesis of 2, 2'-(1, 3-dithiolan-2-ylidenemethanediyl) diquinoline-4-carboxylic acid [s1]

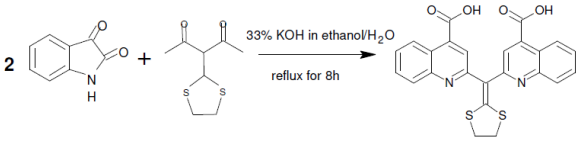

Scheme – 2

Isatin (1mmol) was added to a solution of 33% of KOH in water, after the reaction mixture was added to (2.1mmol) of 3-(1,3-dithiolan-2-ylidene)pentane-2,4-dione) and the reaction mixture was heated for 8 hours. After that the reaction mixture was cooled to room temperature and acidified with 1N HCl until the reaction mixture reaches to pH=3. Then it was kept for overnight and the resulted mixture was filtered, washed for 2-3 times in water and pet-ether and finally the residue was purified by silica gel chromatography(chloroform: methanol 9:1 v/v) yield :72%. 1H NMR (DMSO-d6, 400 MHz): 13.7 (s, 2H, COOH), 8.6 (d, 2H pyridine 3c–H) and for benzene 8.0 (d, 2H, Ar–H), 7.9 (d, 2H, Ar–H), 7.78 (t, 2H, Ar–H) 7.6 (t, 2H, Ar-H), and aliphatic protons at 3.54 (4 H,s). MS: m/z = 458.9 (M-1).

2.5. Preparation of ZnO nanoparticles

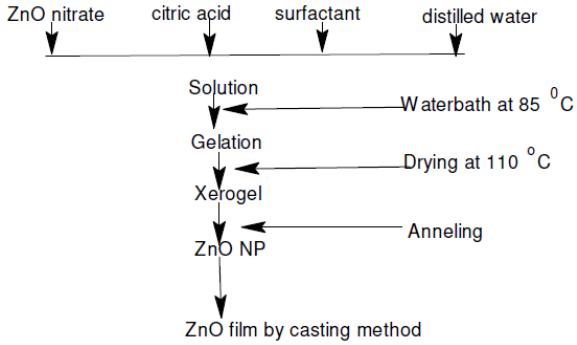

Scheme – 3

2.6. Preparation of ZnO films

The prepared non-agglomerated different sized ZnO nanoparticles were ground in a porcelain mortar with a small amount of water (0.5ml) containing acetyl acetone to prevent re-aggregation of the particles. After the particles had been dispersed by the high shear forces in the paste, it was diluted by slow addition of water (1.5ml) under continuous grinding. Finally a surfactant (Triton X-100, Aldrich) was added to facilitate the spreading of the colloid on the substrate and then the paste was spread uniformly using a smooth glass stick with the draw rate around 2 cm/s. The thickness of the ZnO film was controlled by adhesive tape (thickness ~ 5 μm) surrounding the square film area. The films were heated at 450°C for 1h to decompose the organic paste between ZnO particles.

2.7. Growth of the organism

Liquid cultures of E. coli (Escherichia coli ATCC 25922) were grown aerobically in Luria Broth (LB) at 37º C on a rotary shaker (170 rpm) for 18 hrs. The cells were centrifuged at 6000 rpm at 4ºC for 5 min and suspended in 5 ml phosphate buffer solutions (PBS).

2.8. Light source

A 100W tungsten halogen lamp was used. The irradiation light was filtered with a filter that cut off the light with wavelength below 420 nm.

The intensity of the illumination was 10 $mWcm^{-2}$ on the catalyst surface during the experiment.

2.9. Irradiation and experimental procedures

The cell suspension was diluted 105 times and then 2 ml of the diluted cell suspension was pipette onto the coated ZnO films. For each sample, 20 µl cell solution was extracted by a pipette and spread on to the petri-dish containing LB culture medium followed by incubation for 24 h at 37º C and then finally the number of colonies on the dishes were counted.

3. RESULT AND DISCUSSION

3.1. XRD studies

The X-ray diffraction data were recorded by using Cu Kα radiation (0.15406 nm). The intensity data were collected over a 2θ range of 20-60 º**.** The average grain size of the samples was estimated with the help of Scherer equation using D = Kλ/β COSθ, here K is constant, λ is the wavelength of X-ray radiation employed (1.54056 Å), β is corrected full width at half maximum and θ is Bragg angle. From the figure 1 shows that the XRD patterns of ZnO nanoparticles were corresponding to hexagonal wurtzite structure and all the diffraction peaks were in good agreement with the reported JCPDS card no. 89-139. No other characteristic peaks were observed other than ZnO nanoparticles and the obtained average crystallite size was about 10-50 nm. Experimental work reports that by varying the pH and citric acid concentration affects the grain size of the ZnO nanoparticles. Y.L.Zhang, et.al reported that low aggregative ZnO nanoparticles were obtained at the optimized citric acid concentration is in the ratio of C Zn2+/Ccit = 1:1.5. [23]. In our experiments, the effects of pH on the average grain size of the ZnO nanoparticles were estimated from XRD peaks as shown in figure 1A. It was observed that grain sizes of the ZnO particles were minimal and the surface area was maximal at a pH 1. This was because the citric acid was incompletely ionized without NH_3. H_2O and acted as a bridge between two Zn2+ ions to form a three-dimensional complex [26]. The grain size was increased as ammonia was added drop wise to the solution to adjust the pH below 7. A lower NH_3 H_2O/ Zn $(NO_3)_2$ molar ratio resulted in increased super saturation of the solution. Consequently, a great deal of ZnO precipitate was obtained from the solution by homogeneous nucleation in a short time, which inhibited the growth of the ZnO nanoparticles and led to a decrease in the ZnO grain size at a pH of 7. It was theorized that Zn2+ was stably complexed by ammonia for a high NH_3 H_2O/Zn $(NO_3)_2$ molar ratio. As a result, heterogeneous nucleation of ZnO seldom occurred and the particles grew slowly [27] as shown table 1.

The obtained ZnO nanoparticles were decorated on glass substrate and characterized by XRD spectra's is as shown in Figure 1B. A series of characteristic peaks are observed, and they are in accordance with the hexagonal wurtzite phase of ZnO crystalline peaks (JCPDS card no 89-139). No peaks of impurities were observed, suggesting that the high purity ZnO nanocrystalline films was obtained. In addition, the peak is widened little at pH =1 ZnO nanocrystalline film implying that the particle size is small according to the Debye–Scherer formula D= Kλ/(βcosş) and the other characteristic peaks are still in accordance with the hexagonal wurtzite phase of ZnO films. The average crystallite size of the prepared different pH of ZnO nanocrystalline films as listed given in table 2.

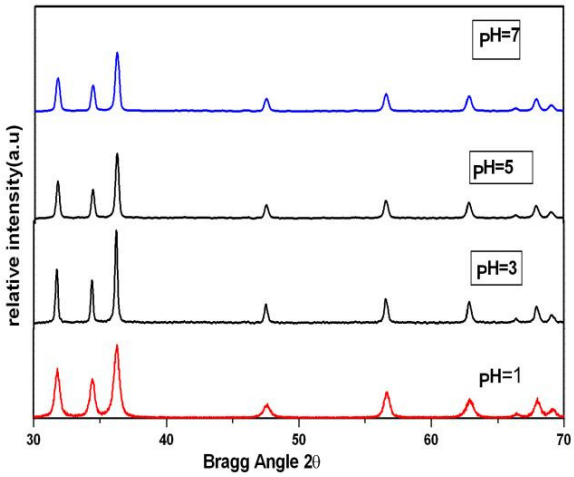

Figure – 1A: XRD spectra's of different grain sized (A) ZnO nanoparticles and (B) ZnO nanocrystalline films (a) pH =1 (b) pH =3 (c) pH =5 and (d) pH =7.

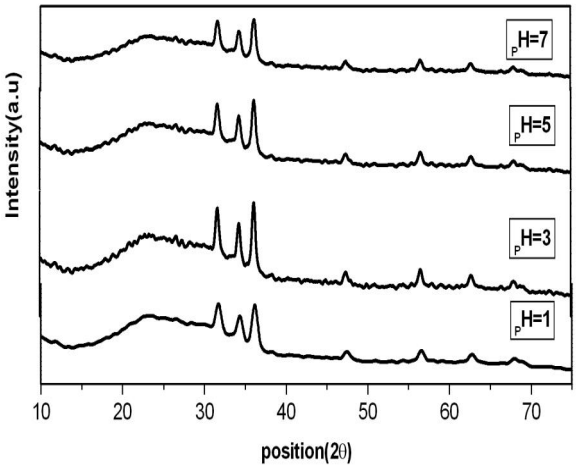

Figure – 1B: XRD spectra's of different grain sized (A) ZnO nanoparticles and (B) ZnO nanocrystalline films (a) pH =1 (b) pH =3 (c) pH =5 and (d) pH =7.

Table -1: Surface area and grain size of ZnO nanoparticles prepared at a pH of 1, at a pH of 3, at a pH of 5, and at a pH of 7

pH values	Conc. Citric acid	Average grain size(nm) ZnO particles	Surface area by BET using nitrogen (m^2g^{-1})
pH=1	1:1.5	10	75
pH =3	1:1.5	48	16
pH =5	1:1.5	34	21.4
pH =7	1:1.5	29	26.78

Table -2: Surface area and grain size of ZnO nanocrystalline films prepared at a pH of 1, at a pH of 3, at a pH of 5, and at a pH of 7

pH values	Conc. citric acid	Average grain size(nm) of the ZnO films
pH =1	1:1.5	15
pH =3	1:1.5	53
pH =5	1:1.5	39
pH =7	1:1.5	32

3.2. Photo-physical properties

Figure 2 shows that absorption spectra of the different grain sized ZnO nanocrystalline films shows the absorption peaks at 380, 374, 370 and 365 nm respectively for pH of 1,7,5 to pH of 3, which shows that by varying pH the wavelength shifts towards lower region. The optical properties are strongly dependent on the particle size i.e. blue shifted with respect to the bulk absorption edge appearing at 380 nm [28]. It is clear that the absorption edge systematically shifts to the lower wavelength or higher energy with decreasing size of the nanocrystalline films. This pronounced and systematic shift in the absorption edge is due to the quantum size effect [29]. As known large particle showed a smaller surface area and void volume which influences a much higher light scattering ability than that of the small nanocrystalline films [30]. Hence, from the obtained absorbance the ZnO nanocrystalline films prepared at pH =3 and pH =5 are having high intensity then the absorbance spectra of ZnO nanocrystalline films prepared at pH =1 and pH =7 this is due to light scattering effect.

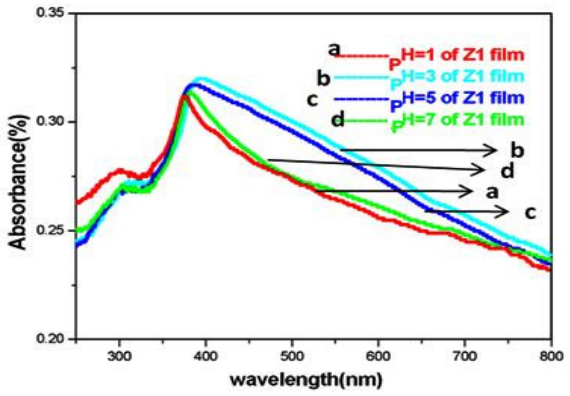

Figure - 2: UV-Visible absorbance spectra of different sized ZnO nanocrystalline films.

In figure 3 shows an attempt of preliminary study on the adsorption of S1 sensitizer containing carboxylic acid groups on the surface of ZnO crystalline films recorded on absorption spectra using ethanol solutions of dyes before and after the chemisorbtion of ZnO films. The considerable amount of shift in the absorption spectrum of the dye molecules upon binding to the nanocrystalline films can be explained in terms of complex formation as well as charge transfer transitions via electron transfer between ZnO and the dye molecule, which results in the considerable red shift due to relaxation of the energy levels of the dye. This is in agreement of similar results which was previously reported [31, 32].

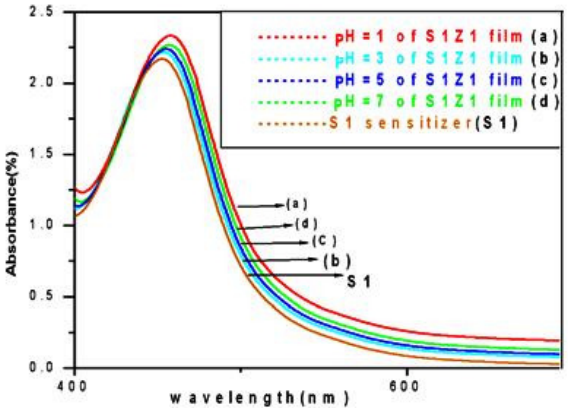

Figure - 3: UV-Visible absorbance spectra of different sized S1 sensitizer functionalized ZnO nanocrystalline films

The obtained experimental results shows that pH = 1 and pH = 7 of ZnO nanocrystalline films functionalized with S1 sensitizers increases the absorbance and shifting band at longer wavelength (3nm) indicates a electronic coupling

and a charge transfer type of interaction between the S1sensitizer and ZnO nanocrystalline films. Similarly at pH = 3 and pH = 5 shows same behavior, but it is less than the above grain sized films. This is mainly causes because of smaller grain sized nanoparticles is directly proportional to larger surface area, which offers higher chemisorbtion of dyes over monolayer films.

3.3. ATR-IR spectra of S1-sensitizer and S1-ZnO film

Major IR bands of free S1 sensitizer are as follows: 1710.3 cm^{-1} for C=O stretching mode; 1380.1 cm^{-1} for the symmetric stretching of CO_2; 1156.2 cm^{-1} for COH bending; 1241.3 cm^{-1} for singly bonded C O stretching, Instead, there is an broad band at 1606.9 cm^{-1} which was assigned to the antisymmetric stretching of CO_2^-, where the negative charge is delocalized to give two equivalent (or nearly so) C-O bonds. The IR spectrum of S1 sensitizer adsorbed on ZnO was little changed in the region 1300-1700 cm^{-1}. The most prominent change was the band at 1704 cm^{-1} (ν(C=O)), whose intensity was greatly reduced by chemisorbed ZnO nanocrystalline films. The intense broad band at 1602 cm^{-1} which is assigned to the antisymmetric stretch of CO_2^-, This indicates that the surface complexes of S1 sensitizer were attached through a bidentate coordination (BC),but not through a monodentate coordination (MC) [35].The band at 1143 cm^{-1} ((C-O H)) was also absent upon adsorbing on ZnO films, which further confirms the bidentate surface complex formation.

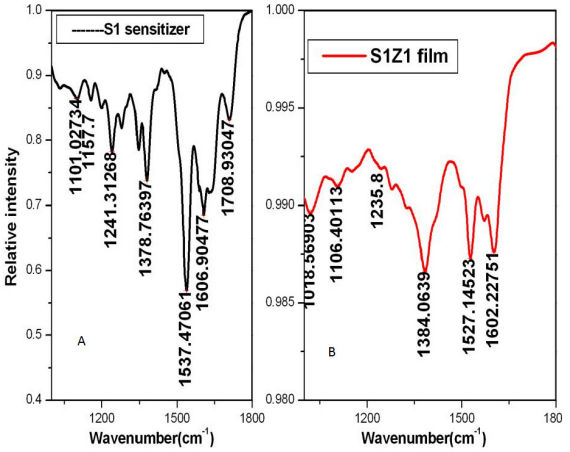

Figure – 4: ATR-IR spectral studies of [A] 2,2'-(1,3-dithiolan-2 ylidenemethanediyl) diquinoline-4-carboxylic acid and[s1] and [B] S1 sensitizer chemisorbed on ZnO film.

3.4. H1NMR and Mass spectra of S1 sensitizer

From the figure 5 It was observed that the 1H NMR spectra of the ligand exhibited the multiplet in the region δ 7.5-7.98 ppm is assignable to aromatic protons of benzene ring, two proton at δ 8.54 ppm is assignable pyridine ring (doublet), four aliphatic protons δ 3.4 ppm (singlet) is assignable as $-CH_2$ protons and in the region δ 14.1 ppm (singlet) assignable to carboxylic proton (broad).

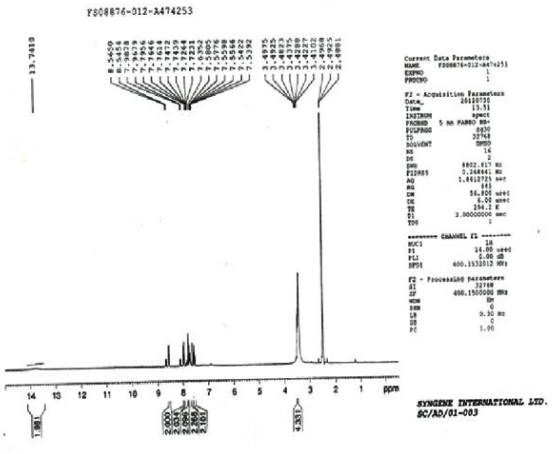

Figure - 5: H1NMR spectra S1 sensitizer.

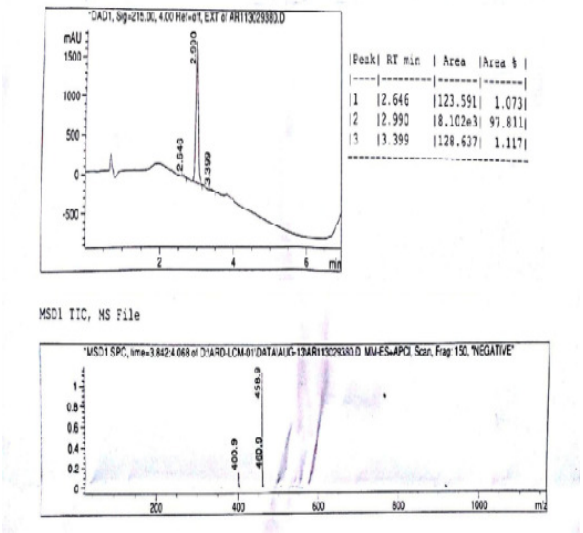

Figure - 6: Mass spectra of S1 sensitizer.

The mass spectra were analysed in LC-Mass, the compound showed [M^{-1}] molecular ion peak. The mass spectra of novel sensitizer were presented in Figure.6 respectively, it shows that the molecular ions represent the base peaks in the spectra and so reflect their stable nature under electron impact. The base peak of obtained compound was m/z =458.9 (M-H).

3.5. Antibacterial studies

By introducing immobilization of the photocatalyst several factors that influence the efficiency of the photocatalytic inactivation of microbes may be changed such as the access of light and oxygen to the photocatalyst surface, the distance between microbes and photocatalyst and possible penetration of the photocatalyst nanoparticles into microbe cells [36]. Although photoinactivation of bacteria should be more

efficient in suspensions of a photocatalyst as compared to its immobilized form. The latter has a particular advantage as the immobilized photocatalyst may form a self disinfecting and self-cleaning surface. Therefore, in our experiments the photoinactivation of bacteria was tested in the presence of immobilized visible light activated by functionalized ZnO films. Searching for surfaces easily self-disinfectable upon illumination with typical light sources as a result we decided to use a halogen lamp instead of a high pressure mercury lamp. The spectrum of the light emitted by a halogen lamp resembles the spectrum of diffuse daylight more than that emitted by a high pressure mercury lamp. It comprises only a very small part of UV-light necessary for direct excitation of unmodified ZnO film. These, S1/ZnO sensitizer films whose photoactivation effect of E. coli. bacteria were tested in the presence of visible light source. Apparently, under the experimental conditions immobilized form of the photocatalyst instead of suspension, significantly lower the photocatalytic activity because of the induced oxidative stress appeared to be insufficient for an effective bacteria inactivation.

The photo-assisted bactericidal effects of the dye-sensitized films on E. coli cells were tested under visible light source was filtered with a cutoff light wavelength below 420 nm. The survival ratios of the bacterial cells in the system of ZnO nanocrystalline film and sensitizers under visible light irradiation does not changes. These results indicate that pure ZnO nanocrystalline films alone or the dye alone has no apparent bactericidal activity under the corresponding experimental conditions as shown in figure 7. These S1-sensitized ZnO films have higher bactericidal activities than ZnO nanocrystalline films. About 42-55 % of the E. coil cells were killed in 1 h on the ¿lm prepared by S1 sensitizer chemisorbed on different grain sized ZnO nano crystalline films figure 7. (curve a- d). The bactericidal activity decreased a little bit for the film prepared with S1 chemisorbed large sized ZnO nano crystalline films because of the coverage of the dye on the surface of ZnO films is lesser than the S1 chemisorbed small sized ZnO nano crystalline films. Hence to explore the optimum condition to achieve photo-inactivation of bacterial cells under visible irradiation will be the objective of the present work. The absorbance Intensity and wavelength of the films is dependent on the generation of oxidative radicals for bactericidal inactivation. Similar observations have been reported Ying-Chan Hsu. et.al in the field of dye-sensitized solar cells showing that their energy conversion were dependent on the amount of dyes adsorbed and lack of absorption beyond >600 nm [37]. Therefore pH=1 of S1 chemisorbed ZnO nano crystalline films shows higher photocatalytic activity as compared to the other pH leveles prepared ZnO nano crystalline films due to higher the surface area affects higher the chemisorbtion of sensitizers.

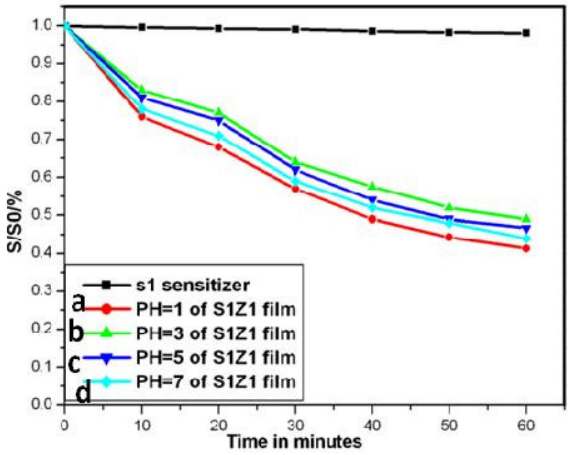

Figure – 7: E-coli survival ratio of S1 sensitized molecule adsorbed on different grain sized ZnO nano films under visible light irradiation.

4. CONCLUSION

This paper presents the visible light induced photoactivity of functionalized Zinc oxide crystalline films in the processes of E-coli bacteria killing. A significant effect of visible light illumination was observed in S1 sensitizer adsorbed Zinc oxide crystalline films than bare ZnO films. The maximum photo inactivation requires relatively high visible light dosages, Hence smaller grain sized ZnO films chemisorbs higher the amount of S1 sensitizer which achieves the higher bactericidal effect as compared with other films. i.e. at pH =1, showed a shift in the wavelength and absorbance Intensity towards higher region then the other pH levels (3,5,7) prepared ZnO nanocrystalline films due to the smaller the grain size is directly proportional to larger surface active sites which offers higher the chemisorbtion of sensitizers on ZnO nanocrystalline films.

Acknowledgement

PNP tanks to the Department of chemistry, Kuvempu University, Karnataka, india and HRR thanks to the Principal and staff of PG Department of Physics and research centre, Bharathicollege, Bharathinagara, Mandya District in Karnataka State, India for permitting to carry out this research work.

5. REFERENCES

1. Curridal ML, Comparelli R, Cozzli PD, Mascolo G and Agostiano A. **Mater. Sci. Eng. C.** 2003; 23: 285.

2. Kamat VP, Huehn R and Nicolaescu R. **J. Phys. Chem. B.** 2002; 106: 788.
3. Wang ZS, Huang CH, Huang YY, Hou YJ, Xie PH, Zhang BW and Cheng HM. ***Chem. Mat.*** **2001;** 13: 678.
4. Cherepy NJ, Smestad GP, Gratzel M and Zhang JZ. **J. Phys. Chem. B**. 1997;101: 9342.
5. Petrella A, Cozzoli PD, Curri ML, Striccoli M, Cosma P and Agostiano A. **Bioelectrochemistry.** 2004; 63: 99.
6. Kay A and Graetzel M. **J. Phys. Chem.** 1993; 23: 6272.
7. Benjamin S, Vaya D, Punjabi PB and Ameta SC. **Arabian J. Chem.** 2011; 4: 205.
8. Zyoud A. Ph.D.Thesis, **An Najah National University, Palestine,** 2009; 155.
9. Fujishima A and Honda K. **Nature.** 1972; 238: 37.
10. Hoffmann MR, Martin ST, Choi W, Bahnamann DW. **Chem.Rev.** 1995; 95: 69.
11. Yu JC, Lin J, Lo D and Lam SK. **Langmuir.** 2000; 16: 7304.
12. Huang Z, Maness PC, Blake DM, Wolfrum EJ, Smolinski SL, Jacoby WA. **J. Photochem. Photobiol. A. Chem.** 2000; 130: 163.
13. Matsunaga T and Okuchi M. **Environ. Sci. Technol.** 1995; 29: 501.
14. Jing Liqiang, Wang Dejun, Wang Baiqia, Li Shudan, Xin Baifu, Fu Honggang, Sun Jiazhong. **J. molecular Catalysis. A.** 2006; 244: 193.
15. Hagfeldt A and Gratzel M. **Chem. Rev. 1995;** 95: 49.
16. Lenzmann F, Krueger J, Burnside S, Brooks K, Gratzel M, Gal D, Ruhle S and Cahen D. **J. Phys. Chem. B.** 2001; 105: 6347.
17. Nazeeruddin MK, Pechy P, Renouard T, Zakeeruddin SM, Humphry Baker R, Comte P, Liska P, Cevey L, Costa E, Shklover V, Spiccia L, Deacon GB, Bignozzi CA and Gratzel M. **J. Am. Chem.Soc. 2001;** 123: 1613.
18. Haque SA, Tachibana Y, Willis RL, Moser JE, Gratzel M, Klug DR, Durrant JR. **J. Phys. Chem. B.** 2000; 104: 538.
19. Bach U, Lupo D, Comte P, Moser JE, Weissortel F, Salbeck J, Spreitzer H and Gratzel M. **Nature.** 1998; 395: 583.
20. Cho YM, Choi WY, Lee CH, Hyeon T and Lee HI. **Environ. Sci. Technol.** 2001; 35: 966.
21. Sondos Othman and Abed Alhadi Ateeq. ***Thesis*****. 2012** ; 1.
22. Dieter RK. **Tetrahedron.** 1986; 42, 3029.
23. Zhang YL, Yang Y, Zhao JH, Tan RQ, Cui P and Song WJ. **J Sol-Gel Sci Technol.** 2009; 51: 198.
24. Hardy A, Haen JD, Van Bael MK and Mullens J. **J Sol–Gel Sci Technol.** 2007; 44: 65.
25. Yu K, Jin ZG, Liu XX, Liu ZF and Fu YN. **Mater Lett.** 2007; 61: 2775.
26. Virendra P, Charlnene D, Deepti Y, Shaikh AJ and Nadanathangam V. **Spectrochemica Act part A,** 2006**;** 65: 173.
27. Soosen Samuel M, Lekshmi Bose and George KC. **Acedamic Review.** 2009; 1: 57.
28. Munkhbayar B, Dorjderem M, Sarangerel D and Bayanjargal Ochirkhuyag. **Nanosci. Nanotechnol. Lett.** 2013; 5: 1.
29. Nazeeruddin MK, De Angelis F, Fantacci S, Selloni A, Viscardi G, Liska P, Ito S, Takeru B, Graetzel M. **J. Am.Chem. Soc.** 2005; 127: 16835.
30. De Angelis F, Fantacci S, Mosconi E, Nazeeruddin MK and Graetzel M. **J. Phys. Chem. C.** 2011; 115: 8825.
31. Kim Finnie S, John Bartlett R and James Woolfrey L. **Langmuir.** 1998; 14: 2744.
32. Srinivasan C and Somasundaram N. **Curr. Sci.** 2003; 85: 25.
33. Ying Chan Hsu, Hegen Zheng, Jiann T'suen Lin and Kuo-Chuan Hoa. **Solar Energy Materials & Solar Cells. 2005;** 87, 357.